

# Competing Magnetic Phases on a “Kagomé Staircase”

G. Lawes,<sup>1</sup> M. Kenzelmann,<sup>2,3</sup> N. Rogado,<sup>4</sup> K. H. Kim,<sup>1,†</sup> G. A. Jorge,<sup>1</sup> R. J. Cava,<sup>4</sup> A. Aharony,<sup>5</sup> O. Entin-Wohlman,<sup>5</sup> A. B. Harris,<sup>6</sup> T. Yildirim,<sup>3</sup> Q. Z. Huang,<sup>3</sup> S. Park,<sup>3,7,§</sup> C. Broholm,<sup>2,3</sup> and A. P. Ramirez<sup>1,8</sup>

<sup>1</sup> Los Alamos National Laboratory, Los Alamos, NM 87544

<sup>2</sup> Department of Physics and Astronomy, Johns Hopkins University, Baltimore, MD 21218

<sup>3</sup> NIST Center for Neutron Research, Gaithersburg, MD 20899

<sup>4</sup> Department of Chemistry and Princeton Materials Institute, Princeton University, Princeton, NJ 08544

<sup>5</sup> School of Physics and Astronomy, Raymond and Beverly Sackler

Faculty of Exact Sciences, Tel Aviv University, Tel Aviv 69978, Israel

<sup>6</sup> Department of Physics and Astronomy, University of Pennsylvania, Philadelphia, PA, 19104

<sup>7</sup> Department of Materials Science and Engineering,

University of Maryland, College Park, MD 20742 and

<sup>8</sup> Bell Labs, Lucent Technologies, 600 Mountain Avenue, Murray Hill, NJ 07974

(Dated: November 15, 2020)

We present thermodynamic and neutron data on  $\text{Ni}_3\text{V}_2\text{O}_8$ , a spin-1 system on a kagomé staircase. The extreme degeneracy of the kagomé antiferromagnet is lifted to produce two incommensurate phases at finite  $T$  – one amplitude modulated, the other helical – plus a commensurate canted antiferromagnet for  $T \rightarrow 0$ . The  $H - T$  phase diagram is described by a model of competing first and second neighbor interactions with smaller anisotropic terms.  $\text{Ni}_3\text{V}_2\text{O}_8$  thus provides an elegant example of order from sub-leading interactions in a highly frustrated system.

PACS numbers: 75.10.Jm, 75.25.+z, 75.30.Kz

Geometrical magnetic frustration leads to unusual low temperature spin order and dynamics and presents new challenges for the theoretical understanding of magnetic systems. Frustrated materials are often characterized by triangle-based lattices and short-range antiferromagnetic (AF) interactions.<sup>1</sup> Of particular interest has been magnetism on the two-dimensional (2D) kagomé lattice, which consists of corner-sharing triangles. While the Heisenberg spin-1/2 model appears to have short range spin correlations and a gap to free spinons,<sup>2,3</sup> the  $S \rightarrow \infty$  classical model has Néel order with a  $\sqrt{3} \times \sqrt{3}$  unit cell at temperature  $T = 0$ .<sup>4</sup> Materials that approximate the kagomé AF can be expected to lie close to a quantum critical point, and indeed early work on the kagomé system SCGO exposed a spin liquid phase possessing a large fraction (15%) of the total spin entropy and short range  $\sqrt{3} \times \sqrt{3}$  order.<sup>5,6</sup> Later work on jarosite systems showed different “ $q = 0$ ” long range order apparently favored by interlayer interactions.<sup>7</sup>

Here we study  $\text{Ni}_3\text{V}_2\text{O}_8$  (NVO) in which the  $S = 1$   $\text{Ni}^{2+}$  spins form the orthorhombic kagomé staircase structure shown in Fig. 1(a).<sup>8</sup> This structure has the coordination and two-dimensionality of the regular kagomé lattice, but the kagomé planes are buckled. The system is particularly attractive because its complex magnetic phase diagram can be understood on the basis of an embellished kagomé spin hamiltonian. The model we introduce also applies to the isostructural compounds where Ni is replaced by Cu<sup>9</sup> or Co.<sup>10</sup> Although the symmetry of these compounds is the same as that of NVO, their phase diagrams are very different. As indicated below, this difference results from a small quantitative change in the parameters which dictate how frustration is relieved.

A previous study of the magneto-thermal response in

polycrystalline NVO revealed four zero field phase transitions with  $\Theta_W/T_N > 5$ , where  $\Theta_W$  is the Weiss constant and  $T_N$  the magnetic ordering temperature.<sup>10</sup> In this letter we report an unexpectedly rich anisotropic field-temperature ( $H - T$ ) phase diagram (Fig. 2), with high and low temperature incommensurate (IC) phases (HTI and LTI) and two commensurate (C and C') spin structures. These magnetic structures are determined via neutron diffraction. We also explain the salient features of NVO by a model, in which the spine ( $\text{Ni}_s$ ) and cross-tie ( $\text{Ni}_c$ ) spins interact via nearest neighbor (NN) and second nearest-neighbor (SNN) isotropic Heisenberg interactions. In addition, and consistent with crystal symmetry, it is necessary to take account of the Dzyaloshinskii-Moriya (DM) interaction and magnetic anisotropy.

Symmetry is key to understanding the ordered phases that spring from the kagomé critical state in NVO.<sup>11</sup> In the presence of AF ordering on the spine sites, isotropic NN interactions produce zero mean field on cross-tie sites. In this regard, NVO is reminiscent of  $\text{Sr}_2\text{Cu}_3\text{O}_4\text{Cl}_2$ <sup>12</sup> and of some “ladder” systems of recent interest.<sup>13</sup> However, the structural anisotropy of NVO induces interactions not usually considered in frustrated systems. First, because the  $\text{NiO}_6$  octahedra are edge-sharing, the NN Ni-O-Ni bond angle is close to  $90^\circ$  so the NN and SNN Ni-Ni interactions are weak and similar in strength. Second, the symmetry of the crystal structure admits a DM interaction among the NN spine spins.<sup>12</sup> Third, anisotropic pseudo dipolar (PD) exchange interactions between spine and cross-tie spins induce both a uniform and a staggered moment on the cross-tie sites.<sup>14</sup> These interactions add to the usual isotropic NN super-exchange interaction to produce the observed rich  $H - T$  phase diagram.

Single crystals of NVO were grown from a  $\text{BaO-V}_2\text{O}_5$

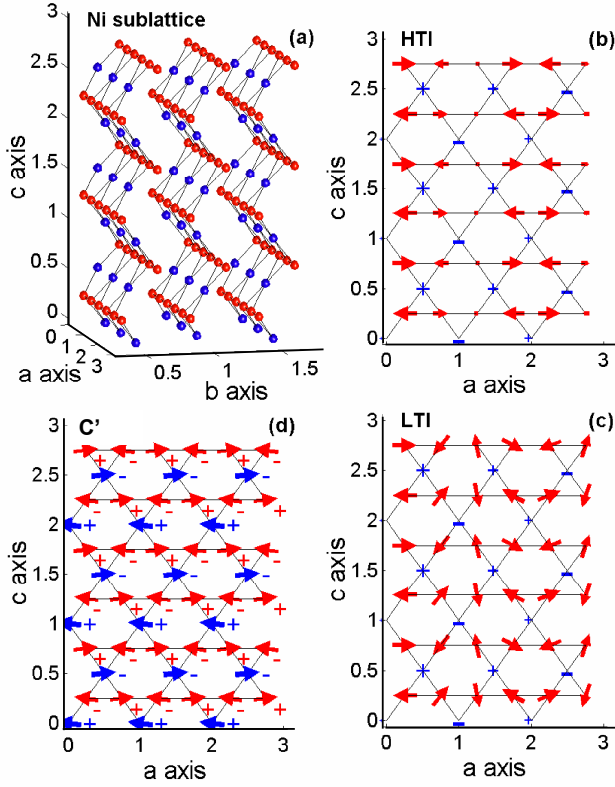


FIG. 1: (a) Structure of NVO, showing the cross-tie  $Ni_c$  (blue (gray)) and spine  $Ni_s$  (red (black)) sites. (b)-(c) indicate the spin structures in the incommensurate phases. + and - indicate spin components along  $\mathbf{b}$ . Symbol sizes scale with the dipole moment. (d) indicates the symmetry of the low  $T$  commensurate spin structure. Spin canting has been exaggerated for clarity and the relative symbol sizes for spine and cross tie spins are not to scale. Subsequent layers are displaced by  $(\mathbf{a} + \mathbf{b})/2$  with spine spins satisfying Eq. (1). Lattice parameters serve as axis length units.

flux and powder samples were synthesized with standard techniques.<sup>10,14</sup> The uniform magnetization,  $M$ , was probed using a commercial SQUID magnetometer. The specific heat,  $C$ , was measured with a commercial calorimeter using the relaxation method for  $T > 2$  K and the semi-adiabatic method for lower  $T$ . Powder and single crystal neutron diffraction measurements were carried out at the NIST Center for Neutron Research.<sup>14</sup> The space group of NVO is  $Cmca$  (No. 64)<sup>8</sup> with lattice parameters  $a=5.92197(3)$  Å  $b=11.37213(7)$  Å, and  $c=8.22495(5)$  Å at  $T = 1.5$  K. Throughout we index wave vectors in the orthorhombic reciprocal lattice with  $a^* = 2\pi/a$ ,  $b^* = 2\pi/b$ , and  $c^* = 2\pi/c$ . Representative specific heat data are in Fig. 3(a) for a magnetic field ( $H$ ) of 0, 5, and 8 T along  $\mathbf{c}$ . As in previous zero field measurements on powder samples, there are four peaks in  $C(T)$ .<sup>10</sup> The entropy reduction associated with these phase transitions is determined by  $\Delta S = \int_0^{50K} (C/T)dT$ , after subtracting an estimate of the lattice contribution obtained from the non-magnetic structural analog  $Zn_3V_2O_8$ . We find  $\Delta S \approx 7.9$  J/mole K, or 87% of  $R\ln 3$ , which is close to

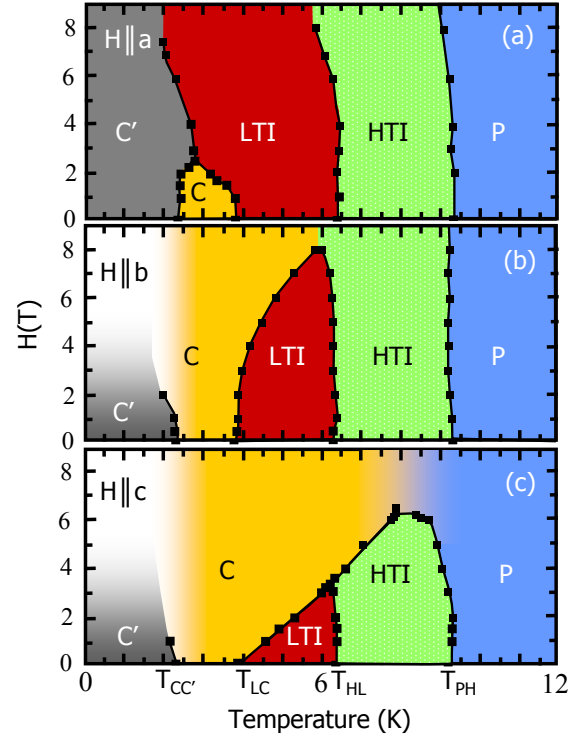


FIG. 2: Phase diagram for NVO as a function of temperature and magnetic field applied along the three principal crystallographic directions. For  $\mathbf{H} \parallel \mathbf{c}$  no true phase boundary separates the P and C phases. White areas were not probed.

that expected for ordering among spin-1  $Ni^{2+}$  ions. We infer that the specific heat peaks mark phase transitions to unique structures involving the  $Ni^{2+}$  spin-1 degrees of freedom. The  $H = 0$  peaks at 2.2 K, 6.3 K, and 9.1 K indicate second order phase transitions, whereas the 3.9 K peak marks a first order transition.

Through extensive specific heat measurements, we determined the phase boundaries shown in Fig. 2. These were confirmed by susceptibility ( $\chi$ ) and magnetization measurements (see Fig. 3(b)), which provide additional clues to the nature of the phases. The susceptibility exhibits significant magnetic anisotropy. As  $T$  is reduced and the C phase is entered, there is a sharp jump in  $M$ , up to 3.5% of the  $Ni^{2+}$  saturation moment for  $\mathbf{H} \parallel \mathbf{c}$ , which indicates a weak ferromagnetic (FM) moment along  $\mathbf{c}$ . With  $\mathbf{H} \parallel \mathbf{a}$ , there is a sharp drop in  $M$ . Finally, for  $\mathbf{H} \parallel \mathbf{b}$ , there is no sharp feature indicating no FM moment along  $\mathbf{b}$ . A surprising result of this study is that the  $T_{PH}$  and  $T_{HL}$  transitions do not produce observable anomalies in  $\chi(T)$ . In a field of 0.1 T the magnetization anomaly at  $T_{PH}$  is less than  $4 \times 10^{-5} \mu_B/Ni$  or 0.3% of the signal while it is less than  $4 \times 10^{-6} \mu_B/Ni$  or 0.03% at  $T_{HL}$ . Nonlinear susceptibility measurements likewise produced no indication of these phase transitions.

Neutron diffraction, however, reveals temperature dependent magnetic Bragg peaks at  $\mathbf{Q} = (2n + 1 \pm q/a^*, 2m + 1, 0)$  and  $\mathbf{Q} = (2n + 1 \pm q/a^*, 2m + 1, 2m + 1)$

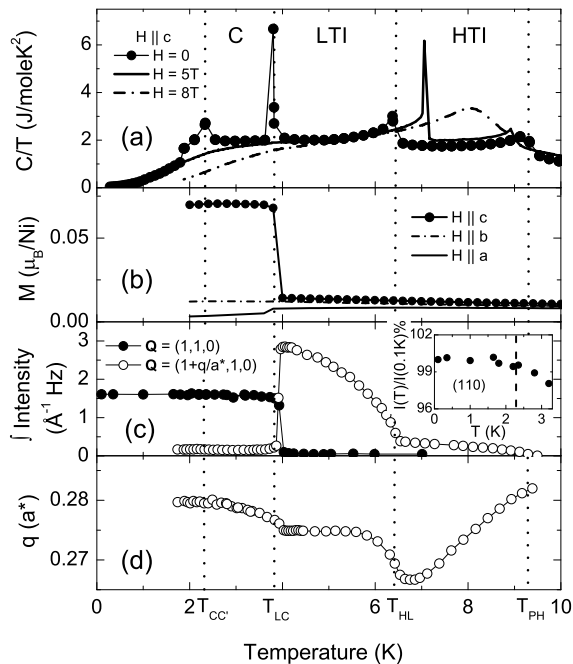


FIG. 3: (a) Specific heat of NVO, in zero field and for  $H \parallel c$ . (b) Longitudinal magnetization versus  $T$  for  $H = 0.1$  T along the three principal crystallographic directions. (c) Integrated intensity of commensurate and incommensurate magnetic Bragg peaks at  $\mathbf{Q} = (110)$  and  $(1 \pm q/a^*, 1, 0)$ , respectively. (d) Temperature dependence of the incommensurate magnetic wave vector. In the C and C' phases we believe the incommensurate peak reflects a meta-stable minority phase as it is only present after cooling through the HTI and LTI phases and can be fully suppressed by field cycling.

for  $T_{LC} < T < T_{PH}$ . The peaks are resolution limited indicating a correlation length in excess of 500 Å. The  $T$ -dependence of the peak intensities is shown in Fig. 3(c). Anomalies are apparent at the three high  $T$  transitions,  $T_{PH}$ ,  $T_{HL}$ , and  $T_{LC}$ , and the peaks vanish in the  $H = 0$  paramagnetic (P) phase. The absence of an anomaly to the level of 0.5% (see inset) in the  $T$ -dependence of the (110) magnetic Bragg peak through the phase transition at  $T_{CC'}$  indicates that this transition involves degrees of freedom that are decoupled from the prevailing AF order. Fig. 3(b) shows that the weak FM moment is also unchanged through this transition. Nonetheless we believe the specific heat anomaly at  $T_{CC'}$  is intrinsic as it was observed in all samples studied (1 powder and 5 crystals).

The  $T$ -dependence of the characteristic magnetic wave vector,  $q$ , is shown in Fig. 3(d). Again there are anomalies at all the upper transitions but not at  $T_{CC'}$ . In phases HTI and LTI,  $q$  varies continuously indicative of an IC magnetic structure. The C phase is commensurate though cooling through phases HTI and LTI yields a metastable remnant of the IC modulation. To determine the spin structures in the HTI, LTI, and C' phases we collected zero field (ZF) magnetic Bragg intensity data for 170 peaks in the (hk0) and (hkk) planes at  $T = 7$  K, 5 K, and for 70 peaks at  $T = 0.1$  K after ZF cooling. We

analyzed the data using group theoretical classification of the possible spin structures.<sup>15</sup>

In the HTI phase, we limited consideration to magnetic structures that form a single irreducible representation of the corresponding space group, because we reject the possibility of a multicritical point where more than one irreducible representation simultaneously become critical.<sup>15</sup> Irreducible representation  $\Gamma_4$ <sup>14</sup> provides an excellent account of the HTI phase with a reliability coefficient  $R=17\%$ . The corresponding magnetic structure is illustrated in Fig. 1(b). At  $T = 7$  K the wavelength of the a-modulated structure is  $\lambda_m = 2\pi/(a^* - q) = 1.37(1)a$  with an amplitude vector  $\mathbf{m}_s^4 = (1.12(4), 0.04(9), 0.01(8)) \mu_B$  for spine spins and  $\mathbf{m}_c^4 = (0, -0.3(1), 0.00(6)) \mu_B$  for cross-tie spins. There is a phase shift of  $0.4(2)\pi$  between the IC waves on the two sublattices.

The LTI phase contains an additional irreducible representation,  $\Gamma_2$ , for the  $\mathbf{c}$  component of spine spins (Fig. 1(c)). For  $T = 5$  K the spine spin amplitudes are  $\mathbf{m}_s^4 = (1.04(8), 0.0(1), 0.01(6)) \mu_B$  and  $\mathbf{m}_s^2 = (0, -0.01(6), 0.76(7)) \mu_B$ . The wavevectors for the two components were experimentally indistinguishable and the phase shift of  $0.3(1)\pi$  indicates an elliptical spiral in the  $\mathbf{a} - \mathbf{c}$  plane. The cross-tie amplitude is  $\mathbf{m}_c^4 = (0, -0.8(4), 0.1(1)) \mu_B$  with a phase shift of  $0.5(2)\pi$  to  $\mathbf{m}_s^4$ . There is no detectable cross tie spin component associated with irreducible representation  $\Gamma_2$ :  $\mathbf{m}_c^2 = (0.0(1), 0, 0) \mu_B$ . The reliability coefficient was  $R = 22\%$ .

In the low temperature commensurate C' phase the data are consistent with the spin structure shown in Fig. 1(d) which corresponds to a mixture of representations  $\Gamma_1$  and  $\Gamma_7$ . While the spine sublattice is fully polarized:  $\mathbf{m}_s^1 = (0, 0.29(8), 0) \mu_B$  and  $\mathbf{m}_s^7 = (2.28(6), 0, 0.1(4)) \mu_B$ , this is not the case for the cross tie sites where  $\mathbf{m}_c^1 = (-0.26(8), 0, 0) \mu_B$  and  $\mathbf{m}_c^7 = (0, 0.3(1), 0.1(8)) \mu_B$ . In this fit the total magnetization along  $\mathbf{c}$  was fixed to the value of  $0.05 \mu_B$  per Ni atom as determined from bulk magnetization measurements. The reliability coefficient was  $R = 11\%$ . Having two active representations in C' indicates that  $T_{CC'}$  could mark the admixture upon cooling of  $\Gamma_1$ . This scenario is, however, difficult to reconcile with the absence of an anomaly in the  $T$ -dependence of the (110) Bragg intensity (inset to Fig. 3(c)).

We now turn to a theoretical interpretation of these results. First, note that the dominant AF component of the spine magnetization in all  $H = 0$  phases satisfies

$$\mathbf{m}(\mathbf{r}) = -\mathbf{m}(\mathbf{r} \pm \frac{1}{2}\mathbf{b}) = -\mathbf{m}(\mathbf{r} \pm \frac{1}{2}\mathbf{c} + \delta\mathbf{b}), \quad (1)$$

where  $|\delta| = 0.26048(6)$ <sup>8</sup> accounts for the kagomé plane buckling. This indicates AF interactions between neighboring spines. The spin-structure within spines is controlled by competing NN and SNN isotropic Heisenberg interactions denoted  $J_1$  and  $J_2$ . A mean field treatment<sup>16</sup> indicates that for  $J_2 > |J_1|/4$  the spine Hamiltonian is minimized by a mean field spin modulation with wave vector,  $q$ , which satisfies  $\cos((a^* - q)a/2) = -J_1/(4J_2)$ . Putting aside the small  $T$ -dependence of  $q$ , we deduce

from the experimental value ( $q \approx 0.27a^*$ ) in the LTI and HTI phases that  $J_1 \approx 2.6J_2$ . In the presence of easy-axis anisotropy the highest-temperature ordered phase is predicted,<sup>16</sup> in agreement with our experiments, to be a longitudinally modulated phase in which the spins are confined to the easy  $\mathbf{a}$  axis. If the anisotropy field  $H_A$  is not too large ( $H_A < H_1$ ), then, as the temperature is lowered the longitudinally modulated phase gives way to one in which an additional transverse modulated component of spin appears, growing continuously from zero as the LTI phase is entered. This scenario is also consistent with our diffraction data. At still lower temperature the diffraction data indicate the presence of a commensurate AF phase. According to mean-field theory, such a transition can occur for sufficiently large anisotropy,  $H_A > H_2$ .<sup>16</sup> Our numerical mean field calculations<sup>17</sup> show that for  $J_1/J_2 = 2.6$  indeed  $H_1 > H_2$ , so that there is a range of anisotropy field for which mean field theory predicts the observed sequence of ZF phase transitions.

We now discuss some of the finer details of these phases. From the  $M$  versus  $H$  data, extrapolated to  $H = 0$ , we find that in the C phase there is a weak ferromagnetic moment. Structural considerations show that the DM interaction for a single spine takes the form

$$\mathcal{H}_{\text{DM}} = \sum_n [D_c \mathbf{c} + (-1)^n D_b \mathbf{b}] \cdot [\mathbf{S}(n) \times \mathbf{S}(n+1)] \quad (2)$$

where  $n$  labels the spins consecutively along the spine.  $D_b$  gives rise to a linear coupling between the staggered moment of the spine along  $\mathbf{a}$  and the weak ferromagnetic moment of the spine along  $\mathbf{c}$ . This weak ferromagnetic moment can induce a ferromagnetic moment along  $\mathbf{c}$  on the cross-tie spins via isotropic Heisenberg exchange. In addition, such a moment on the cross-tie spins can also arise via PD interaction between the staggered moment on the spines and a uniform moment on the cross-tie spins. Symmetry also admits a staggered g-tensor along the spines, the physical origin and consequences of which are similar to DM interactions.<sup>18</sup> The weak ferromagnetism explains the absence of a phase boundary between the P and C phase for  $\mathbf{H} \parallel \mathbf{c}$ . In the IC phases, these inter-

actions would give rise to modulated moments along  $\mathbf{c}$ . The anisotropic interactions we invoke also generate couplings between the various IC order parameters, which result in weak  $T$ -dependence of the IC wave vector.<sup>17</sup>

Next we discuss the phase boundaries between the C phase and the IC phases. Barring a multicritical point, these must be first order transitions. For  $\mathbf{H} \parallel \mathbf{c}$  the Zeeman energy,  $-HM$ , of the FM moment (in the C phase) explains why the transition temperatures  $T_{LC}$  and  $T_{HC}$  increase linearly with increasing  $H$ . For  $\mathbf{H} \perp \mathbf{c}$  the Zeeman energy does not appear and the phase boundary of the C phase should be quadratic in  $H$  [ $T_N(H) = T_N(0) + \alpha H^2$ ] as it depends on the differences in the susceptibilities of the phases involved. In particular, when  $\mathbf{H} \parallel \mathbf{a}$ , the longitudinal susceptibility of the C phase is small and the coefficient  $\alpha$  is negative, disfavoring the C phase. The other phase boundaries ( $T_{PH}$  and  $T_{HL}$ ) are also expected to be quadratic in  $H$  and the experimental phase diagrams are consistent with this although for the HTI phase when  $\mathbf{H}$  is along  $\mathbf{b}$ , the coefficient  $\alpha$  is unusually small. This fact is linked to the absence of anomalies in  $\chi$  at the HTI phase boundaries. Both features may be a consequence of a frustrated and weakly connected spin system where phase transitions occur from a strongly correlated state with short range AF order.

In summary, we have studied the phase diagram of the spin-1 kagomé staircase  $\text{Ni}_3\text{V}_2\text{O}_8$ . We find that although this phase diagram is quite complicated, it can be understood on the basis of a rather simple model which reflects the symmetry of the crystal structure. The experiments and model offer a specific example of how SNN exchange, easy axis anisotropy, and Dzyaloshinskii-Moriya interactions can induce and control complex low temperature phases in a frustrated magnet.

We acknowledge support from the LDRD program at LANL and the U.S.-Israel Binational Science Foundation under grant 2000073 for work at TAU, NIST, UPenn, and JHU. The NSF supported work at JHU through DMR-0306940, work at Princeton through DMR-0244254, and work at SPINS through DMR-9986442 & DMR-9704257. KHK is partially supported by KOSEF through CSCMR.

<sup>†</sup> CSCMR & School of Physics, Seoul National University, Seoul 151-747, S. Korea.

<sup>§</sup> HANARO Center, Korea Atomic Energy Research Institute, Daejeon, S. Korea.

<sup>1</sup> A. P. Ramirez, in Handbook of Magnetic Materials, K. H. J. Buschow, Ed. (Elsevier, Amsterdam), **13**, 423 (2001).

<sup>2</sup> S. Sachdev, Phys. Rev. B **45**, 12377 (1992).

<sup>3</sup> P. Sindzingre *et al.*, Phys. Rev. Lett. **84**, 2953 (2000).

<sup>4</sup> D. A. Huse and A. D. Rutenberg, Phys. Rev. B **45**, 7536 (1992).

<sup>5</sup> A. P. Ramirez *et al.*, Phys. Rev. Lett. **64**, 2070 (1990).

<sup>6</sup> C. Broholm, *et al.*, Phys. Rev. Lett., **65**, 3173 (1990).

<sup>7</sup> A. S. Wills *et al.*, Europhys. Lett. **42**, 325 (1998).

<sup>8</sup> E. E. Sauerbree *et al.*, Acta Cryst. B **29**, 2304 (1973).

<sup>9</sup> N. Rogado *et al.*, J. Phys. Cond. Mat. **15**, 907 (2003).

<sup>10</sup> N. Rogado *et al.*, Solid State Comm. **124**, 229 (2002).

<sup>11</sup> T. Yildirim *et al.*, Phys. Rev. Lett. **72**, 3710 (1994).

<sup>12</sup> F. C. Chou *et al.*, Phys. Rev. Lett. **78**, 535 (1997).

<sup>13</sup> V. Kiryukhin *et al.*, Phys. Rev. B **63**, 144418 (2001).

<sup>14</sup> M. Kenzelmann *et al.*, unpublished (2004).

<sup>15</sup> Yu. A. Izyumov, V. E. Naish and R. P. Ozerov, *Neutron Diffraction of Magnetic Materials*, (Consultants Bureau, New York 1991).

<sup>16</sup> T. Nagamiya, in Solid State Physics, edited by F. Seitz and D. Turnbull (Academic Press, New York), **20**, 346 (1967).

<sup>17</sup> A. Aharony *et al.*, unpublished (2004).

<sup>18</sup> I. Affleck and M. Oshikawa, Phys. Rev. B **60**, 1038 (1999).